SYNERGISTIC METHODS IN REMOTE SENSING DATA ANALYSIS FOR TROPICAL COASTAL ECOSYSTEMS MONITORING

E. C. Paringit [a, b]*, K. Nadaoka [a]

[a] Dept. of Mechanical and Environmental Informatics, Tokyo Institute of Technology,
2-12-1 Ookayama, Meguro-ku, 152-8552, Tokyo, Japan – ecp@wv.mei.titech.ac.jp, nadaoka@mei.titech.ac.jp
[b] Dept. of Geodetic Engineering, University of the Philippines Diliman, Quezon City, 1101- ecp@engg.upd.edu.ph

KEY WORDS: Ecosystem, Integration, Marine, Multisensor, Multitemporal, Multispectral,

ABSTRACT:

Tropical coastal environments around the world have undergone rapid changes which made consequent of their ecosystems degradation inevitable. Despite numerous attempts to map their extent and distribution from space, the ability to relate the surface signals reflected and subsequently measured by remote imaging sensors to the biophysical characteristics of coastal habitat targets have been given inadequate attention. The dynamic characteristic of the coastal shallow water areas including tidal and wave forcing, water quality and environmental stresses, both natural and anthropogenic complicate this task. Hence there is a need to consider these factors in understanding images obtained from different sources taken at various periods. This research focuses on synergistic methods in multi-source image processing for assessing benthic coastal habitats such as corals, seagrass, and algae by examining image data covering these types of environment from space through the aid of theoretical remote sensing approaches. Our study area covers the Fukido river mouth area and Shiraho reef of Ishigaki Island located in southern Ryukus, Japan. Images were acquired from satellite-borne Ikonos, SPOT, ASTER and Landsat respectively in 2002. Principles of BRDF (bidirectional reflectance distribution functions) modelling, shallow water optics and radiative transfer have been utilized to explain shallow water reflectance values with biophysical properties such as distribution, abundance, morphology and depth as controlling parameters. To reinforce parameterizations and to validate computational results, field surveys were conducted to gather *in-situ* data including water quality (mainly chlorophyll-*a* and turbidity), sea surface conditions, benthic habitat cover, abundance and distribution, some of which are synchronous with image acquisition. Spectral profiles across the reef area benthic cover were also used for calibrating reflectance. The developed reflectance model was applied to the image datasets by utilizing model inversion techniques, hence obtaining depth and benthic cover estimates. Results showed relative proximity of image-derived reflectance to processed in-situ spectral reflectance. The accuracy of the cover and depth estimates satellite sensor source image for the same area are also presented. The model provides a physical basis for relating different image datasets from different sources.

1. INTRODUCTION

1.1 Background on Remote Sensing of Coastal Habitats

Due to recurrent global climate anomalies and increased habitation in coastal zone, tropical marine environments around the world have undergone abrupt and undesirable changes. Reckless utilization of coastal resources resulted in deterioration of their nurtured habitats (coral reefs, seagrass meadows and mangrove stands). In order to expediently devise proper conservation measures and formulate sustainable management alternatives for these coastal ecosystems, there is a need first to develop means to obtain reliable information on the state of their health and well-being, and thereafter provide tools to continuously monitor them.

Attempts to map the extent and distribution of coastal marine habitats from space data are numerous and are already near pervasion. Activities, however has been confined merely for mapping shallow benthic coverage on a piecemeal and intermittent mode. Regardless of restrictions cost and weather conditions, the application of conventional remote sensing analysis approaches to any single satellite data (e.g. IKONOS, Landsat TM, SPOT) in current operation barely go beyond classification accuracy above 70% (Mumby and Edwards., 2002).

In terrestrial and global fields, immense interest has been devoted in taking advantage of the repetitive acquisition capability of remote sensors for discriminating landcover features and for detecting associated changes (Coppin, 2004). Over tropical coastal habitats, the ability to combine these sources and make inferences from a multitude of image sources are met with immense challenge due to a number of considerations inherent to sensor systems and those that are attributed to the nature of coastal environment.

1.2 The need for synergistic approach

It is hypothesized that combination of images coming from various sources may lead to improved performance of feature extraction and classification. This paper outlines a method for combining imagery from different sensors that would yield a compatible product useful for processing them in the context of extracting resource information in coastal zones. To date, the ability to relate the surface signals reflected and subsequently measured by remote imaging sensors to biophysical characteristics of coastal habitat targets remain elusive. A compounding difficulty in spectrally resolving habitat features is that the dynamic nature of the coastal shallow water areas including tidal and wave forcing, water quality and environmental stresses, both from natural and anthropogenic

* Corresponding author.

origins, alter spectral properties of benthic cover. Hence there is a need to consider these factors in understanding images obtained from different sources taken at various periods.

2. SITE, DATA AND PROBLEM APPROACH

The goal of synergy is to reconcile all imagery into a common resolution without loss of detail necessary to accomplish classification and feature tasks. The first step is to convert nominal radiance values measured by each satellite sensor into a single standardized reflectance image dataset with the basic criteria that corrections must be rooted on theoretical grounds. Reflectance detected by each sensor is rectified according to acquisition date and time, imaging geometry: these two acquisition conditions regulate incoming radiant energy and modulate reflectance. Since water depth governs light penetration, tide level conditions are accounted for carefully as it changes even among images acquired by a single sensor. Coastal habitats are further complicated by the dynamic nature of the water column. Optically-active constituents present in the water modify tone and pigmentation are therefore modelled. To compare reflectance values from satellite sensors with that of *in-situ* instruments such as field spectroradiometers, the spectral response functions of the sensors per band range are taken into account.

2.1 Target sites and field spectral measurements

There are two areas selected for this study: Shiraho Reef (24°21'N, 124°15'E) and Fukido River mouth area (24°29'N, 124°13'E). Both are located in Ishigaki Island, Southern Ryukus. Shiraho Reef typifies a subtropical fringing reef (Figure 1) and abundant with almost 200 coral species. On the other hand, the moat area reef area outside Fukido River is notable for mixed seagrass beds in abundant cover. Five cross-shore (5) transect lines in Fukido River mouth and another five (5) Shiraho Reef area were established. The average length of the transects in Fukido is about 200 meters while the transects in Shiraho is approximately 400 meters. Depths along these transects reaches 25 meters but are about 1-3 meters on the average. The cross-shore transect configuration allows for sampling of all possible shallow benthic cover on the two types of shallow reef areas.

Onboard a small motor boat, a portable dual-channel spectroradiometer (Ocean Optics S2000®: spectral resolution 2058 pixels equivalent to 332 nm to 1016nm range) was used to gather horizontal spectral profiles along the transects. The sensor of one channel is equipped with a glass diffuser and focused vertically upward. We designate this as the *sun* sensor. On the other hand, the sensor of the other channel (*object sensor*) directed vertically downwards, is submerged and attached to a buoy. The buoy is left to float about 4 meters away from a boat so the latter casts no shadow over the bottom cover being measured by the former. The boat is then driven along the transects while a portable computer continuously logs the spectral data channel and location from a GPS (Global Positioning Systems) unit at 5-km/hr average speed. At 300ms This speed enabled acquisition of spectra at 3 scans per meter.

Ground truth data were collected for the same transect lines where the spectral measurements were obtained. Field data obtained include position, depth (both by echosounder and line measurements), benthic cover, coral, seagrass and algae distribution in Jul 2002 and Aug 2003. Above and below-water PAR sensors were used to measure in-water solar irradiance.

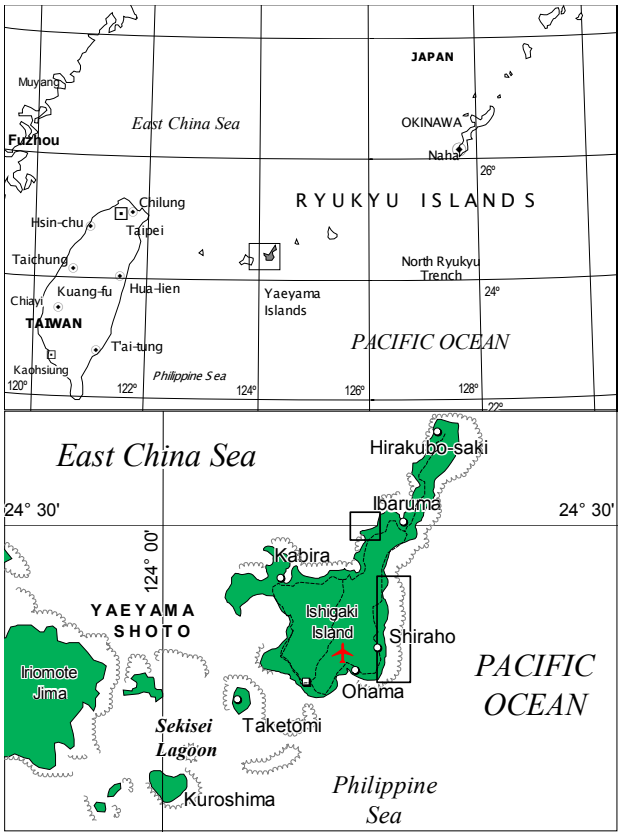

Figure 1. Location of field sites for this study. Above: vicinity of Ishigaki Island. Below: upper block show Fukido area, lower rectangular block covers Shiraho Reef area.

2.2 Satellite images

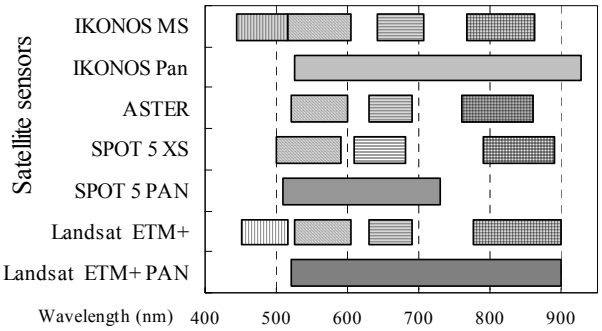

Figure 2. Summary of spectral sensitivity ranges of sensors used for this study.

One scene from each of the multispectral sensors of SPOT XS (processing level: Level 2A; spatial resolution: 10m), Ikonos (Geocorrected; 4m), one Landsat ETM+ (2b; 30m) and ASTER (1b: 15m) images were used for this study. Figure 2 illustrates band span ranges of these sensors while Table 1 describes the date, time of acquisition and observation geometry of images. All images were acquired in first quarter of 2002 to reduce seasonal variations across images. Atmospheric correction was applied to all the images by the applying the SPECTRL2 model (Bird and Riordan, 1984) using the solar data from the Ishigaki meteorological station with the same atmospheric column conditions (ozone, aerosol optical depth and water vapour), reducing the values to surface reflectance at sea surface. Subset of the images covering the two target areas (Shiraho: 35 sq km.; Fukido: 4.5 sq. km) were then segregated for further processing.

Table 1. Summary of datasets used for this study

Satellite Sensor	Bands used	Date & time (UTC)	Viewing angle (θ_v)	Sun angle (θ_s)	Azim. diff. ($\lvert\phi_v - \phi_s\rvert$)
Landsat ETM+	1-4	02/23/2002 01:57:21	Nadir	45.04°	136.98°
ASTER VNIR	1-3	02/14/2002-02:32:16	8.59°	51.39°	132.84°
SPOT 5	1-3:	02/07/2003 02:19:26	12.07°	43.42°	123.73°
IKONOS	1-4	03/28/2002 02:25	29.33°	16.70°	20.60°

Next, we address the key issues in merging the datasets in the context of the physical environments at the time of the imaging. We will present a systematic way to refer the spectral and spatial dimensions into a single image plane.

2.3 Spectral data processing

Ideally, when the two spectrometer channels are calibrated to a single standard radiance unit (e.g. in $Wm^{-1}\mu m^{-1}sr^{-1}$) or have pre-cross-calibrated nominal counts, the instantaneous reflectance $R_{obj}(\lambda)$ of an object is the straightforward value of upwelling $E_{obj}(\lambda, obj)$ and downwelling radiance $E_{sun}(\lambda, sun)$ ratio, given that both measurements were taken at the same plane level. For spectrometers of uneven nominal radiance counts, cross-calibration is necessary.

To describe the cross-calibration procedure, we follow the convention $E_{\text{target}}(wavelength, time, sensor)$ for radiances measurements. Let $E_{Sun,}(\lambda, t_1, obj)$ and $E_{ST}(\lambda, t_1, obj)$ be the radiances measured by the object sensor directed upward and of the standard respectively at the same time t_0. However it is physically impossible to obtain such measurement simultaneously with one channel only. Hence the use of another sensor with the same spectral range is necessary. As mentioned, inter-calibration would be needed if channel nominal units do not match $E_{Sun}(\lambda, t_0, sun) = kE_{Sun,}(\lambda, t_0, obj)$ or in general:

$$E_{\text{target}}(\lambda, t_0, sensor1) = kE_{\text{target}}(\lambda, t_0, sensor2), \quad (1)$$

where k is a calibration coefficient, therefore:

$$R_{ST}(\lambda) = k\frac{E_{ST}(\lambda, t_0, obj)}{E_{Sun}(\lambda, t_0, sun)} \quad (2)$$

Typically, the reflectance of the reference standard panel $R_{ST}(\lambda)$ is available (e.g. a Spectralon® or Ever Color®). Our interest then is to find k:

$$k = R_{ST}(\lambda)\frac{E_{Sun}(\lambda, t_1, sun)}{E_{ST}(\lambda, t_1, obj)} \quad (3)$$

When the object sensor is directed at object target, at any time t,

$$R_{obj}(\lambda) = k\frac{E_{Obj}(\lambda, t, obj)}{E_{Sun}(\lambda, t, sun)} \quad (4)$$

Further, if we correct for the effect of the air-water interface by introducing the factor, $\tau = \left[1 - r_F(\theta_s, \theta_v)\right] / n_w^2$ where $r_F(\theta_s, \theta_v)$ is the Fresnel's reflectance due to differences in ray entrance θ_s and exit angles θ_v; n_w is the index of refraction of water (relative to air), and substitute k in Eq. (3), we have the at-surface remote sensing reflectance from a cross-calibrated dual spectrometer:

$$R_{obj}(\lambda) = \left[R_{ST}(\lambda)\frac{E_{Sun}(\lambda, t_1, sun)}{E_{ST}(\lambda, t_1, obj)}\right]\frac{\tau E_{Obj}(\lambda, t, obj)}{E_{Sun}(\lambda, t, sun)} \quad (5)$$

2.4 Depth measurement and correction

A multi-channel echosounder (DE-4000, Biosonics Inc.) equipped with GPS, capable of obtaining depth measurements to an average of 4 soundings per second is installed on a small (4-m length) motor boat. For purposes of tidal correction, a 25-hour tide level measurements was performed by deploying a depth logger (Diver™, Van Essen Instruments) at the reef area in a location with still water conditions during periods where no strong winds are prevailing) to obtain the actual tide amplitudeat time t in a given location within the reef. $\eta(t)$ is then applied to reduce the water depth measurement, $d(t_i)$ at specific time t_i to its average depth, $\bar{d}$ or:

$$\bar{d} = d(t_i) - \eta(t_i) \quad (6)$$

If a satellite imagery was acquired at another period, t_s, then it follows that $d(t_s) = \bar{d} + \eta(t_s)$ or in relation to Eq. (6)

$$d(t_s) = d(t_i) - \eta(t_i) + \eta(t_s). \quad (7)$$

At the time of the satellite image acquisition, no actual amplitude distribution may be available. Instead, an interpolation method may be used based on the predicted tide tables simply by:

$$a(t_s) = a(t_0) + \frac{(t_s - t_0)(\eta(t_1) - \eta(t_0))}{t_1 - t_0} \quad (8)$$

where $\eta(t_1)$ and $\eta(t_0)$ are the inclusive high and low tide magnitudes respectively and $t_0 < t_s < t_1$. While this relationship may also be used to obtain $\eta(t_i)$, measurement of $d(t)$ a single location is necessary to fix the vertical datum.

For purposes of comparison of the field spectral data with image values, we can reduce the spectrometer data measured into band values modulated by the spectral response function:

$$R_{obj}(b) = \frac{\int_{\lambda_{b-start}}^{\lambda_{b-end}} S(b;\lambda) R_{obj}(\lambda) d\lambda}{\int_{\lambda_{b-start}}^{\lambda_{b-end}} S(b;\lambda) d\lambda} \quad (9)$$

where $S(b;\lambda)$ is the relative spectra sensitivity of the sensor for band b at wavelength λ.

2.5 Normalization due to differences in imaging geometry

Previously, Paringit and Nadaoka (2003) studied the biderectional nature of shallow benthic cover reflectance and employed BRDF techniques to infer coral morphological characteristics from both in-situ spectra and satellite signal. BRDF for each benthic cover type was produced based on their pure reflectance $R_{i0}(b)$ and transmittance $\tau_{i0}(b)$ spectra to compute for the normalized reflectance $R_i(b)$, and is applied to each of the reflectance values as:

$$R_i(b) = \frac{2G_v}{3\pi^2}\left[1 - \exp(-0.5F)\right] \times \quad (10)$$
$$2\left[(\pi - \vartheta)\cos\vartheta + \sin\vartheta\right]R_{i0}(b) + (\sin\vartheta - \vartheta\cos\vartheta)\tau_{i0}(b)$$

where ϑ is the scattering angle between incidence (θ_s', ϕ_s) and reflection direction (θ_v', ϕ_v) and expressed as $\cos\vartheta = \cos\theta_v' \cos\theta_s' + \sin\theta_v' \sin\theta_s' \cos(\phi_s - \phi_v)$. Note that the directional parameters (θ_v', θ_s') have been primed to indicate their adjusted value underwater due to refraction effects. The G and F define the morphological characteristics of the benthic cover that are three-dimensional, specifically corals and seagrass. The BRDF for sand is assumed to be Lambertian.

2.6 Fusion of multisource imagery with varying resolution

To fuse images, we employ multiresolution decomposition algorithm (Gross and Schott, 1998; Piella, 2004). This method exploits the fact that the reflectance from the high resolution image bears a linear relationship with its equivalent composite of image pixels of lower resolution. In order to determine the proper relationship, we degraded the higher-resolution satellite data to correspond with the pixel size of lower-resolution satellite data. We then increase the pixel size of the lower resolution image but now weighted according the regressed relationship for the nearest band. In this way, the detail of objects captured in the higher resolution image is preserved while retaining spectral integrity.

Going through all of these procedures, the intermediate product at this stage could now be imagined to be the reflectance 14-band image free from inherent effects of the atmosphere, water surface conditions and object morphology.

2.7 Simultaneous fractional cover, classification and depth estimation

Classification of benthic cover is based on the evaluation of spectral unmixing results and radiative transfer model after the necessary image corrections are accomplished and image fusion is attained (Paringit and Nadaoka 2003). The proportions, f_i of the different benthic cover types are initially deconvolved by a non-negative iterative least squares solution with sum-to-one constraint (NILSSTOC). Using the estimated proportions for the n number of benthic cover, the approximate reflectance is computed by radiative transfer model (RTM):

$$R(b)' = R_\infty(b)\exp(-2k_b d_s) + \left[-1\exp(-2k_b d_s)\right]\sum_{i=1}^{n} f_i R_i(b) \quad (11)$$

where $R_\infty(b)$ is the reflectance at a nearby deep area (outside the reef). The attenuation coefficient k_b also varies only for each band. The depth, d_s initially given, varies with each sensor by the difference $d_s = \bar{d} - \eta(t_s)$. The total rms (root mean square) error, R_t^2 between the approximate reflectance $R(b)'$ and the actual image data $R(b)$ value for m number of bands are then evaluated. We use a downhill simplex method to iteratively vary $\bar{d}$, repeat NILLSTOC and RTM, that will lead to a minimal and stable R_t^2 , The final product of this step therefore will be a set of f_i and the estimated average depth $\bar{d}$.

In the classification, benthic cover is assigned according to its ecological significance (Edinger and Risk, 2000). This scheme is adopted because sometimes it is not necessary to assign benthic cover with the largest f_i for a given pixel. Biological researchers often regard the presence of a certain important habitat as the pertinent cover even if only occurring at a fraction physically.

2.8 Verification and accuracy assessment

In order to check the consistency of the merged datasets, we compared the reflectance spectra of pure benthic cover obtained from the image against the spectral data taken from the field. We also evaluated the relative differences and/or similarities between *in-situ* reflectance transect and its transect representation in equivalent location in the image. We also analyzed the classification and bathymetry estimates based on confusion matrices and statistical measures of errors respectively.

3. RESULTS AND ANALYSIS

3.1 Spectral consistency of merged datasets

Processed data show that there is strong correspondence between the image reflectance and the measured field reflectance (Figure 3). The additional bands augmented appreciably in the recovery of the spectral curves by defining spans of abrupt change in high and low absorption points. Errors seem to be lower on shorter wavelength ranges (9%) especially from targets with naturally high reflectance on the VIS range.

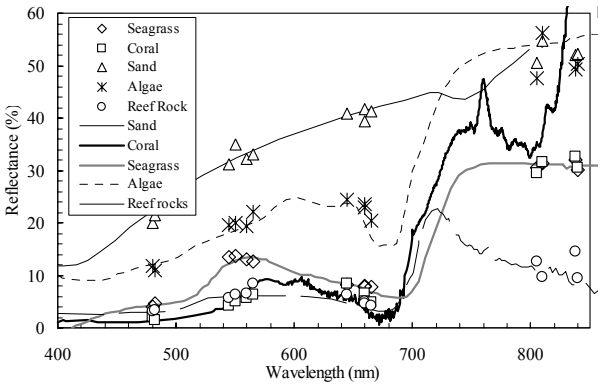

Figure 3. Spectral signatures of typical reef cover types (lines) superimposed with the equivalent reflectance values (marks) obtained from each inclusive band of the satellite sensors used.

As shown in Figure 4, there appears to be a very strong correlation of reflectance values between image and in-situ transects. The strength of the retrievals are significantly reduced (P>0.1) for longer wavelengths particularly the NIR bands.

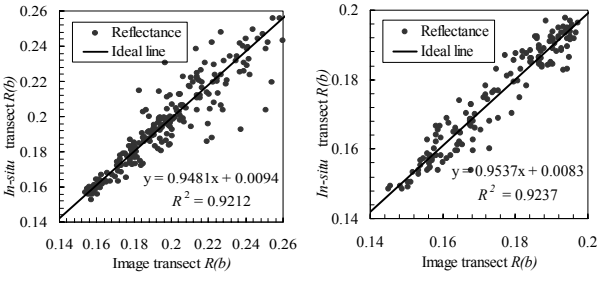

(a) (b)

Figure 4. Comparison of band 1 (IKONOS band 1) reflectance from *in-situ* transects and image transects values along (a) Shiraho Reef: 343 points and (b) Fukido River mouth area: 435 points.

3.2 Analysis of classification results

Ten (10) different band combinations were subjected for classification for 5 coarse types of shallow benthic cover (coral, seagrass, sand, algae, reef rock). In addition, we have also applied the classification procedure for cumulative number of bands in consecutive order of increasing wavelength to assess the effect of systematic increase in band number.

Evaluation of accuracy results indicate that the five band-combination (see Table 2) involving bands 1 of IKONOS and ASTER, bands 2 of Spot and Landsat, and band 4 of IKONOS yields the best result (84.5%). However, this achievement is still comparable (P<0.5) to other five band combinations spanning different band ranges, which are almost identical at 83%. On the opposite end, the classification results from spectrally similar bands from the four sensors produced poorer results (34%, 30% and 28% respectively, in the order of increasing band range), the worst being those bands located in the near infrared (NIR: 780-900 nm) range. It is also observable that higher spatial resolution still commands considerable improvements in overall accuracy except in the case of Landsat ETM+ where it is significantly better that SPOT XS and ASTER VNIR because of the presence of a visible blue band (band centered at 483.2nm). Figure 5 shows the relationship between accuracy and increase in the number of bands corresponding to wavelength.

Table 2. Band combinations, classification performance, and depth estimation accuracy.

Channel number	Classification Accuracy (%)			Depth estimation rms Error*
	Users	Makers	Overall	
3-Band combination ($m = 3$)				
S1, S2, S3	57	54	55.5	0.684
A1, A2, A3	58	59	58.5	0.631
4-Band combination ($m = 4$)				
I2, A1, S1, L1	33	35	34.0	0.39
I3, A2, S2, L3	27	34	30.5	0.28
I4, A4, S3, L4	24	33	28.5	0.31
L1, L2, L3, L4	71	63	67.0	0.36
I1, I2, I3, I4	81	79	80.0	0.25
5-Band combination ($m = 5$)				
I1, I2, S2, S3, S4	74	83	78.5	0.24
L1, I2, L2. S3, L3	81	85	83.0	0.21
I1, A1, S2, L2, I4	80	89	84.5	0.18
All bands ($m = 14$)	79	77	78.0	0.19

Legend: I-Ikonos, L-Landsat ETM, S-SPOT XS, A-ASTER. Number defines channel setting. *Normalized (ratio of rms error to actual depth).

In terms of thematic accuracy, for all classification results, the method delivers best accuracy for sandy areas while there are common difficulties encountered for the seagrass and coral classes. The misclassification of seagrass beds may be attributed to patchy configuration of the meadows, which cannot be accommodated by the input signal coming from the lower-resolution satellite. The problem for coral misclassification arises from confusion in distinguishing them from macroalgae classes. This misinterpretation is ascribed to the presence of symbiotic algae zooxanthella covering the coral itself, which is spectrally similar to macroalgal species such as *Sargassum* sp. and *Lobophora* sp. (Hedley and Mumby, 2002). Overall, classification performed with the spectral unmixing procedure outlined above is generally better than conventional methods (Mumby and Edwards, 2002) applied to individual datasets where accuracies are reported to be lower by more than 5% for coarse habitat mapping.

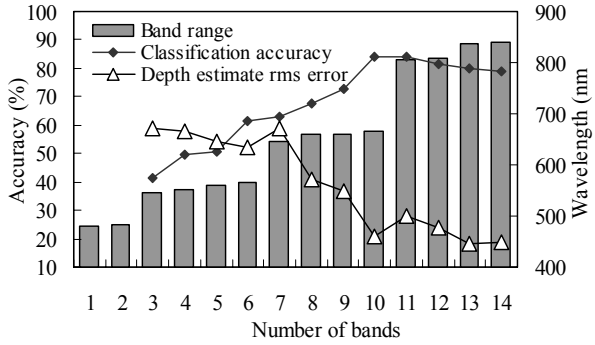

Figure 5. Plot of classification accuracy and depth estimate RMS error with increasing number of bands of longer wavelength.

3.3 Result of bathymetry estimation

Figure 6 illustrates the output bathymetry map for Fukido area using the processed multisource image. It can be seen the model provides a rich topographic detail of a complicated reef system. The presence of the small sand cay areas are well-depicted as well as the abrupt increase in depth at the interface of the reef crest and outer reef flat. Shallow water depths in seagrass and seaweeds are also within realistic range. This is a common pitfall of bathymetry mapping found in conventional approaches like band ratio or regression lines where depth of "darker" bottom cover such as seagrass beds and corals are overestimated.

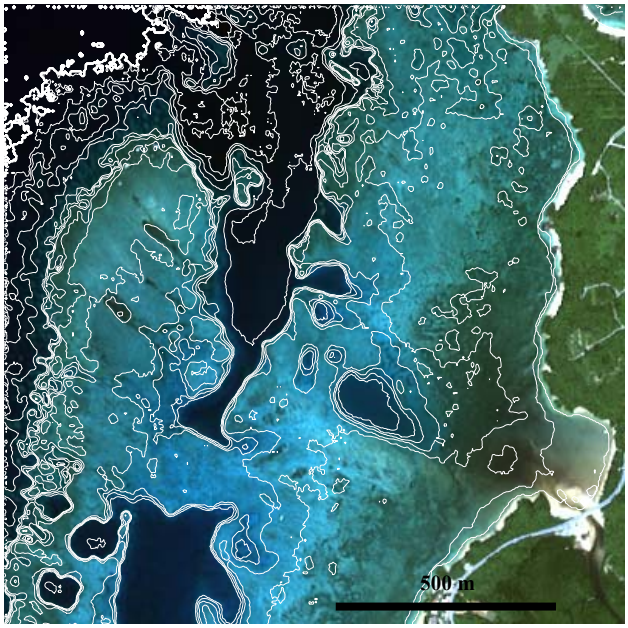

Figure 6. Result of bathymetry estimation (superimposed on IKONOS true-color imager) for Fukido River Mouth area using the fused satellite imagery.

With reference to Figure 5, there appears to be direct relationship between accuracy of depth estimates and the classification correctness. The normalized rms error is reduced to 0.19 when all 14 bands are used and achieves most enhancement with use of the 10th band (Ikonos band 3). The

performance of the estimator begins to deteriorate with the introduction of three more NIR bands. Although it was discerned in the previous section that addition of Landsat ETM+ bands may contribute to better classification results, it also contributed to reduced accuracy in bathymetry estimation.

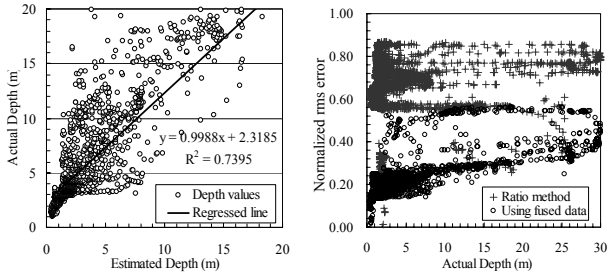

Figure 7. Comparison of estimated and actual depth (left) and normalized rms error on depth estimates against depth (right).

There is a tendency to underestimate depths slightly at shallow areas while discrepancies are much more severe in deeper areas (Figure 7a). This could be caused by uneven spatial distribution of water quality parameters which could not be incorporated in the RTM. We compared the performance of the model against a log-ratio method of two bands (See Stumpf, 2003) and found out that although the error relative to depth is increasing (by 0.20 rms points), the bathymetry estimates are much more accurate than the previous method.

3.4 Discussion

Based on the findings above, we offer the postulate that there is a threshold to classification precision achievable with increasing number of bands, implying that it is sometimes impractical to obtain as much data to process when there is a limit to achievable accuracy. Optimum band placement and spatial resolution are better avenues for improved classification and depth estimates.

Despite the advances made in improving discrimination of reef habitats, some caveats are in order. The procedure relies heavily on the assumption that benthic cover spectral properties remain invariant throughout the acquisition period. Corals and seagrasses are highly dynamic environment and may have change spectra accordingly. There are less minor issues such as anomalies in solar spectrum alterations and satellite drifts which could alter reflectance estimates but should be given careful attention. Image registration is as good only as the GPS used and the surveying technique employed to locate the transects. Also, the method is dependent on a number of physical parameters which could only be obtained by field surveys. It will be difficult to implement the model for areas where prior data or field *in-situ* instruments are not available.

We recommend that evaluation of errors due to image matching misregistration be addressed in future studies. Other promising techniques such as underwater photogrammetric methods, is another worthwhile in attempts to map morphology and bathymetry pursuit given the refined spatial resolution and precise positioning of the acquisition.

4. SUMMARY AND CONCLUSIONS

In this paper, we have presented an approach to spectrally reconcile imageries produced by different sensors and acquired at different dates. We have also presented the benefits and consequences of such synergy in data sources processing methods in discriminating shallow water benthic habitats. This is therefore a clear attempt at synergy, not only of techniques to process images, but also a way to integrate various optical and physical in-situ measurements and their application to radiative transfer modelling to enhance information extraction.

Since typical results from activities where multisource imageries are presented, this paper provides some specific tools and guidelines that planners and decision-makers involved with providing, producing and maintaining information resource on the tropical marine habitats, can have practical use.

ACKNOWLEDGMENTS

We are grateful to Mr Akayoshi Nakayama of the National Research Institute for Fisheries Engineering for providing the IKONOS images. The ASTER images were obtained thru the ARO (Announcement of Research Opportunity Program) of ERSDAC (Earth Resources Data Analysis Center (No. ARO-93). The SPOT images were purchased from support by the Japan Ministry of Environment in monitoring the Sekesei Lagoon National Park, Okinawa while Landsat was furnished by H. Kadoya of NHK.

REFERENCES

Bird, R. E., and Riordan, C. J. 1986. Simple Simple Solar Spectral Model for Direct and Diffuse Irradiance on Horizontal and Tilted Planes at the Earth's Surface for Cloudless Atmospheres." *Journal of Climate and Applied Meteorology*. 25(1), pp. 87-97.

Coppin, P., I. Jonckheere, K. Nackaerts, and B. Muys, 2004. Digital change detection methods in ecosystem monitoring. *International Journal of Remote Sensing*, 42(1), pp. 47-56.

Edinger, E.M and M.J. Risk, 2000. Reef classification bycoral morphology predicts coral conservation value. *Biological Conservation*, 92(1), pp. 1-13.

Gross, H. N. and J. R. Schott, 1998. Application of Spectral Mixture Analysis and Image Fusion Techniques for Image Sharpening. *Remote Sensing of Environment,* 63(2), pp. 85-94.

Hedley, J. D. and P. J. Mumby, 2002. Biological and remote sensing perspectives of pigmentation in coral reef organisms, *Advances in Marine Biology*, 43, pp. 277-317.

Mumby, P.J. and A.J. Edwards, 2002. Mapping marine environments with IKONOS imagery: enhanced spatial resolution can deliver greater thematic accuracy. *Remote Sensing of Environment.* 82(2-3), pp 248-257.

Stumpf, R., K. Holderied, M. Sinclair, 2003. Determination of water depth with high resolution satellite imagery over variable bottom types. *Limnology and Oceanography*, 48(1, part 2), pp 547-556.

Paringit, E. C. and K. Nadaoka, 2003/ Deriving Relationships between Reef Sedimentation and Inland Erosion Characteristics based on field observation data, hydrological modelling and remote sensing data analysis., *Proceedings of the Asian and Pacific Coasts (APAC 2003)*, Tokyo, Japan, March 2004 (in CD-ROM).

Piella, G., 2003. A general framework for multiresolution image fusion: from pixels to regions. *Information Fusion*, 4(3), pp. 259-280.